Supplementary Information

Metal-organic frameworks as conductivity enhancers for all-solid-state lithium batteries

*Shruti Suriyakumar,[a] Rohit M. Manoj,[a] Sreelakshmy K. Jayaprakash, [a] Sreelakshmi Anil Kumar,[a] Keerthy P. Sudhakaran,[a] Vinesh Vijayan [b] and Manikoth M. Shaijumon [a,c]**

[a]School of Physics, Indian Institute of Science Education and Research Thiruvananthapuram, Vithura, Thiruvananthapuram, Kerala 695551, India.

[b]School of Chemistry, Indian Institute of Science Education and Research Thiruvananthapuram, Vithura, Thiruvananthapuram, Kerala 695551, India.

[c]Center for Advanced Materials Research with International Engagement (CAMRIE), Indian Institute of Science Education and Research Thiruvananthapuram, Maruthamala PO, Vithura, Kerala, 695551 India.

* Corresponding Author: shaiju@iisertvm.ac.in

Preparation of composite-Se cathode

Selenium-carbon composite is prepared through a two-step melt diffusion process. ZIF-8 derived Nitrogen-doped carbon was thoroughly grinded and mixed with elemental selenium in 1:2 ratio and the mixture were sealed in an Ar filled autoclave. This is subjected to melt diffusion at 260 ℃ for 12 h and the excess Se is allowed to sublime in a second melt reaction at 280 ℃ for 2 h under flowing Ar to obtain the C/Se with 64% selenium loading.

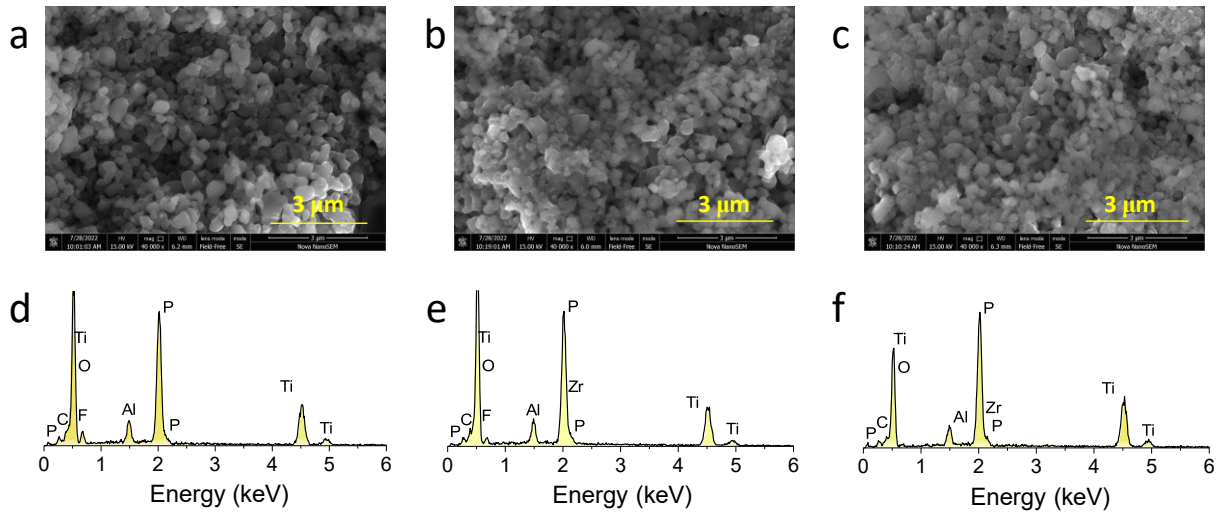

Figure S1. SEM and EDX plot of (a,d) LP (b,e) LPM (c,f) LM pellets, respectively, at the same magnification.

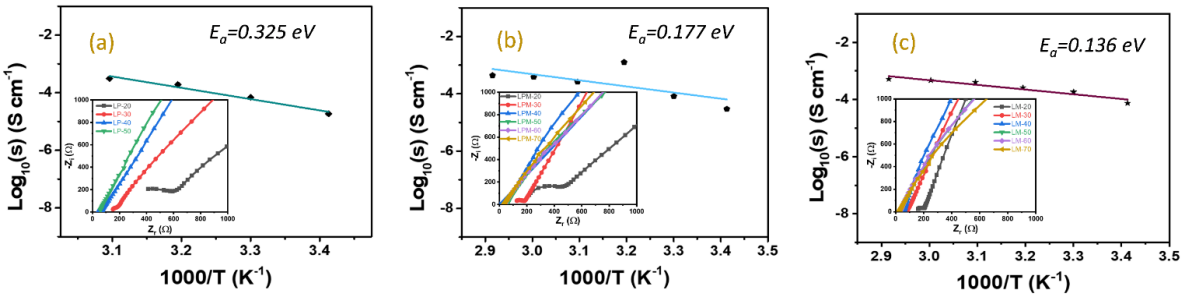

Figure S2. Arrhenius plot of conductivity *vs.* 1/Temperature for the three different pellet compositions (a) LP (b) LPM (c) LM. The inset shows the corresponding Nyquist plots at different temperatures.

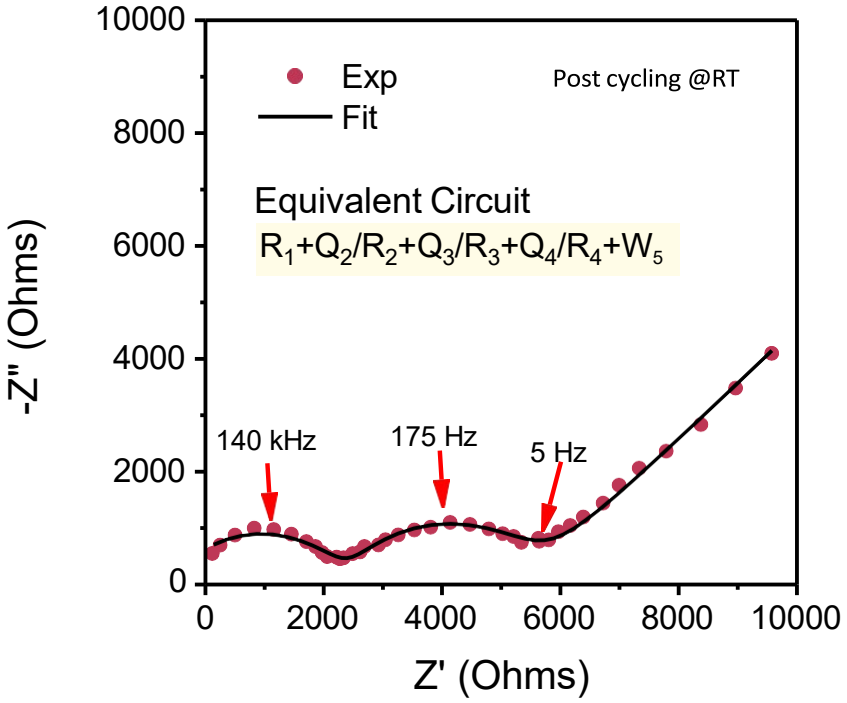

Figure S3. EIS of full cell with LM electrolyte, post cycling.

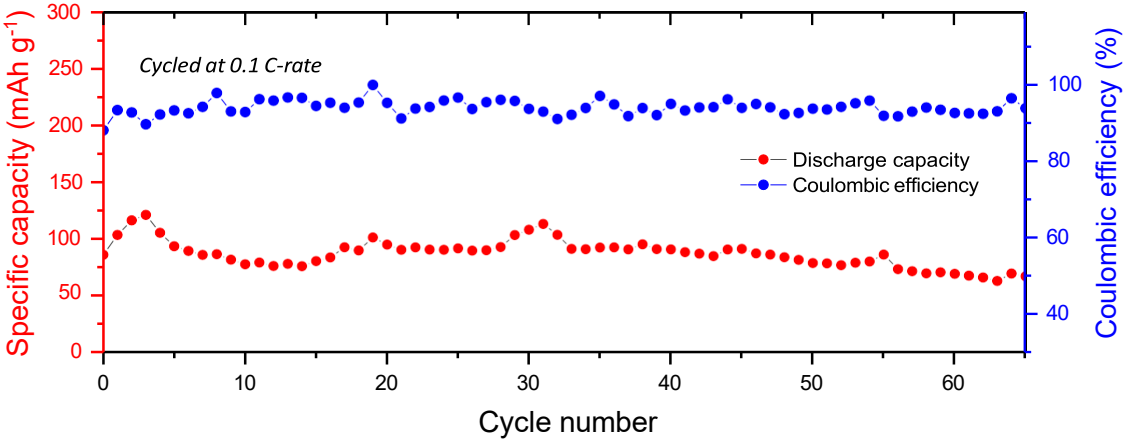

(a)

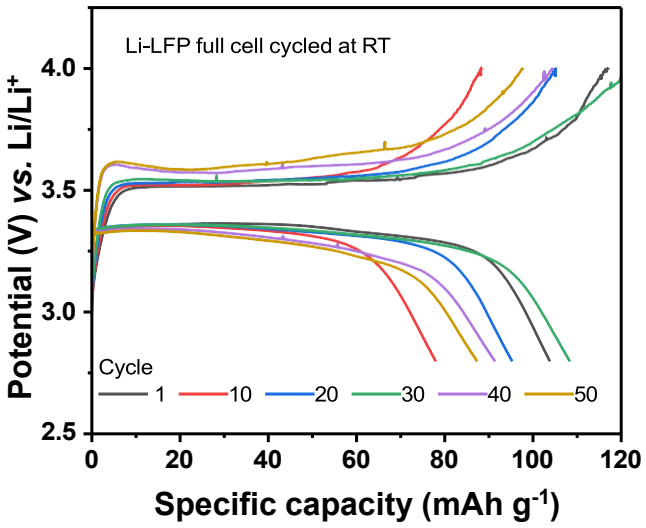

(b)

Figure S4. Cycling stability plot for the full-cell containing LM electrolyte cycled at 0.1 C-rate at RT.

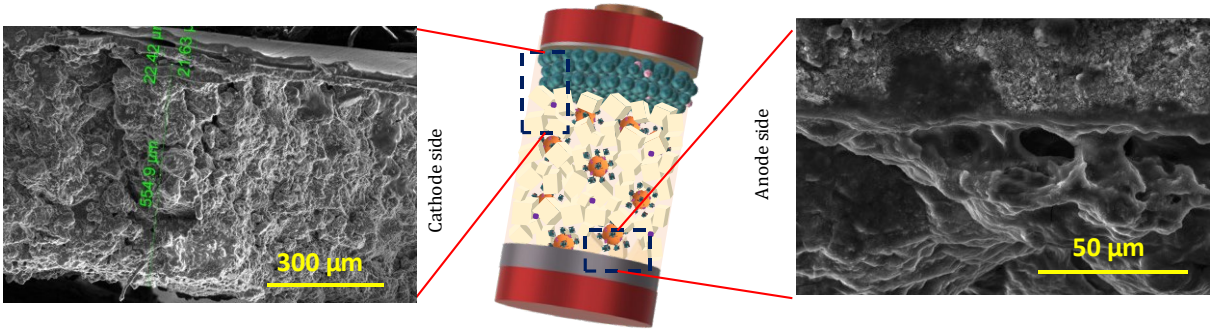

Figure S5. Cross-section SEM image of the electrode-electrolyte interface at the cathode (left) and anode (right) side.

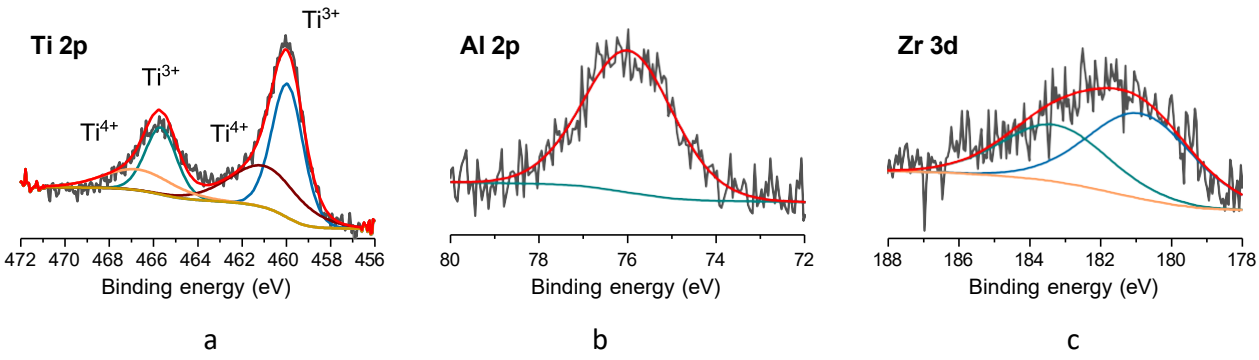

Figure S6. Deconvoluted XPS spectra of the cycled LM electrolyte for (a) Ti 2p, (b) Al 2p, and (c) Zr 3d.

Table S1. Comparison of the electrochemical performance of the LATP +MOF (present work) electrolyte with LATP electrolytes reported in the literature.

Sl. No.	Year	Electrolyte	Modification strategy	Thick-ness	RT Ionic conductivity	Full cell configuration	Cycling capacity @ - rate	Ref
1	2021	LATP	Thin films fabricated by large-area Pulsed Laser Deposition (PLD)	< 1 µm	0.1 m S cm^{-1}	-	-	1
2	2016	LATP/LAGP double-layer solid-state electrolyte	Dry pressing and post-calcination method	55 µm	3.4 * 10^{-4} S cm^{-1}	$LiFePO_4$/LATP–LAGP/Li	145 mAh g^{-1}	2
3	2021	LATP/PVdF−HFP composite	Solution-casting synthesis for new composite solid electrolytes by embedding LATP ceramic into a PVdF−HFP matrix		2.3 × 10^{-4} S cm^{-1}	Li||$LiFePO_4$ with LATP/PVdF−HFP	148 mAh g^{-1}	3
4	2019	LATP	Chemical precursors are mixed and ball-milled, followed by a solid-state reaction and densification through calcination and sintering heat treatments.	1-2 mm	3.5×10^{-4} S cm^{-1}	$LiCoO_2$, $LiFePO_4$, and $LiNi_{0.6}Mn_{0.2}Co_{0.2}O_2$ and Li and $Li_4Ti_5O_{12}$.	147 mAh g^{-1}	4
5	2019	LATP	Effective inhibition of the PEO matrix crystallisation by the high-conductivity LATP nanofillers		1.2×10^{-5} S/cm	$LiFePO_4$/Li	152 mAh g^{-1} at 0.1 C	5
6	2021	(P(VDF-HFP))/(LATP)/P(VDF HFP)	Spray-drying and calcination	21 µm	0.763 mS cm^{-1}	Li/SHSE/$LiCoO_2$	145 mAh g^{-1} at 0.1 C	6
7	2019	LATP	Cold sintering process and post-annealing	300−400 nm	8.04 × 10^{-5} S cm^{-1}	-	-	7
8	2020	LATP ceramic particles and PEO polymer matrix	Sol gel and calcination soln casting	132 µm	1.0 × 10^{-4} S cm^{-1}	Li/CSEs/SS (Li/PEO + LiTFSI/Li, Li/PEO + 15% LATP/Li)	136 mAh g^{-1} 0.1 C	8

9	2022	$Li_{1.3}Al_{0.3}Ti_{1.7}(PO_4)_3$ (LATP) reinforced PEO-PEG-LITFSI composite solid polymer electrolyte (CSPE)	Milling assisted route		10^{-4}–10^{-5} S cm^{-1}			9
10	2019	LATP + PEO polymer and deposited on BN layer.	Sol-gel method+ calcination	0.5–1 mm	$2*10^{-4}$ S cm^{-1}	$LiFePO_4$/LATP/ BN/PEO/Li	142 mAh g^{-1}	10
11	2022	LATP with polyionic liquid binder	Pechini sol-gel , followed by a calcination process		1.2×10^{-3} S cm^{-1}	Li/Li symmetric cell		11
12	2020	LATP-LCO and LATP-LFP	Sol gel	0.13 mm	1.048×10^{-4} S cm^{-1}	Li	C/10 LCO cathode ~ 150 and LFP ~155 mAh g^{-1}	12
13	2019	LATP	Spark Plasma Sintering	40 µm	$1 * 10^{-3}$ S cm^{-1}	N/A	N/A	13
14	2023	PTFE@LATP composite solid electrolytes	PTFE@LATP composite solid electrolytes 3D network made by combining solgel and solid-state grinding methods	100 µm	7.56×10^{-4} S·cm^{-1}	LFP/PTFE@LATP/Li	140.1 mAh·g^{-1} at 1C	14
15	2023	Control sintering temperatures to minimize voids and formation of well-defined grain boundaries	The crystallization temperature was confirmed through TGA/DTA analysis. The degree of crystallization (XRD), the formation of crystal grain boundaries (SEM), and the formation of impurities are examined.	-	1.72×10^{-4} S cm^{-1}	-	-	15

16	2024	Flexible PVDF-HFP@LATP	Simple solution casting method mixing and regulating the ratio of inorganic solid electrolyte and polymer electrolyte	113 µm	2.146×10^{-4} S cm^{-1}	Li/ Flexible PVDF-HFP@LATP/O_2	5314.5 $mAh \cdot g^{-1}$ at 0.1 mA cm^{-1}	16
17	2024	yttrium and silicon co-doped LATP	Conventional solid-state method for co-doping resulting in homogeneous hexagonal morphology and better crystallinity than LATP. 5% LiCl added to it enhances the conductivity significantly.	200 µm	1.88×10^{-4} S cm^{-1}	Li/Li symmetric	-	17
18	2024	LATP-embedded semi-interpenetrating polymer network electrolyte membrane.	Membranes are fabricated by embedding LATP nanoparticles into the semi-interpenetrating network of polyacrylonitrile /poly (ethylene glycol) dimethacrylate (PEGDA).	120 µm	1.06×10^{-3} S cm^{-1}	LFP|HSE|Li	164 mAh g^{-1} at 0.2C	18
19	2024	Polypropylene separators with solid electrolyte LATP and SiO_2 coatings.	LATP mixed PVDF binder was coated onto a PP separator and further applied SiO_2 sol by spin-coating to obtain the PP/LATP/SiO_2 composite separator.	~25µm	0.6×10^{-3} S cm^{-1}	LFP||PP/LATP/SiO_2||Li	~148 mAh g^{-1} at 1C	19
20	2023	LATP+MOF	Cold press with SCN LiTFSI matrix	600 µm	24.7 x 10^{-3} S cm^{-1}	Li/$LiFePO_4$	138 mAh g^{-1} at 0.1 C rate	

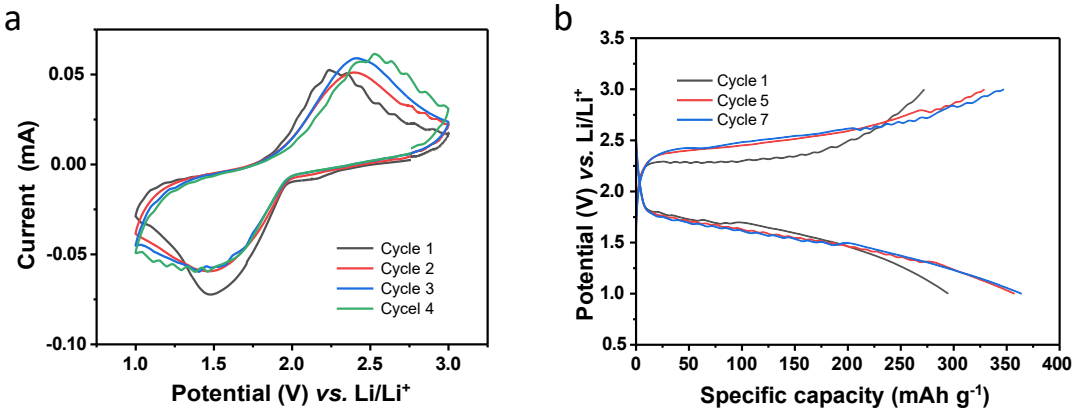

Figure S7. Full-cell studies with carbon-selenium cathode, Li metal anode and LM solid electrolyte at RT (a) CV at 0.2 mV s^{-1} (b) cycling profile of full cells at 0.1 C-rate in coin cell configuration.

Reference

(1) Siller, V.; Morata, A.; Eroles, M. N.; Arenal, R.; Gonzalez-Rosillo, J. C.; López Del Amo, J. M.; Tarancón, A. High Performance LATP Thin Film Electrolytes for All-Solid-State Microbattery Applications. *J Mater Chem A Mater* **2021**, *9* (33), 17760–17769. https://doi.org/10.1039/D1TA02991F.

(2) Zhao, E.; Ma, F.; Guo, Y.; Jin, Y. Stable LATP/LAGP Double-Layer Solid Electrolyte Prepared via a Simple Dry-Pressing Method for Solid State Lithium Ion Batteries. *RSC Adv* **2016**, *6* (95), 92579–92585. https://doi.org/10.1039/C6RA19415J.

(3) Li, Y.; Wang, H. Composite Solid Electrolytes with NASICON-Type LATP and PVdF- HFP for Solid-State Lithium Batteries. *Ind Eng Chem Res* **2021**, *60* (3), 1494–1500. https://doi.org/10.1021/ACS.IECR.0C05075/ASSET/IMAGES/LARGE/IE0C05075_0004.JPEG.

(4) DeWees, R.; Wang, H. Synthesis and Properties of NaSICON-Type LATP and LAGP Solid Electrolytes. *ChemSusChem* **2019**, *12* (16), 3713–3725. https://doi.org/10.1002/CSSC.201900725.

(5) Liu, L.; Chu, L.; Jiang, B.; Li, M. Li1.4Al0.4Ti1.6(PO4)3 Nanoparticle-Reinforced Solid Polymer Electrolytes for All-Solid-State Lithium Batteries. *Solid State Ion* **2019**, *331*, 89–95. https://doi.org/10.1016/J.SSI.2019.01.007.

(6) Kou, Z. Y.; Lu, Y.; Miao, C.; Li, J. Q.; Liu, C. J.; Xiao, W. High-Performance Sandwiched Hybrid Solid Electrolytes by Coating Polymer Layers for All-Solid-State Lithium-Ion Batteries. *Rare Metals* **2021**, *40* (11), 3175–3184. https://doi.org/10.1007/S12598-020-01678-W.

(7) Liu, Y.; Liu, J.; Sun, Q.; Wang, D.; Adair, K. R.; Liang, J.; Zhang, C.; Zhang, L.; Lu, S.; Huang, H.; Song, X.; Sun, X. Insight into the Microstructure and Ionic Conductivity of Cold Sintered NASICON Solid Electrolyte for Solid-State Batteries. *ACS Appl Mater Interfaces* **2019**, *11* (31), 27890–27896. https://doi.org/10.1021/ACSAMI.9B08132/ASSET/IMAGES/LARGE/AM-2019-081322_0002.JPEG.

(8) Huang, Y.; Zhang, Z.; Gao, H.; Huang, J.; Li, C. Li1.5Al0.5Ti1.5(PO4)3 Enhanced Polyethylene Oxide Polymer Electrolyte for All-Solid-State Lithium Batteries. *Solid State Ion* **2020**, *356*, 115437. https://doi.org/10.1016/J.SSI.2020.115437.

(9) Sharma, S.; Singh, M. D.; Dalvi, A. All-Solid-State Electric Double Layer Supercapacitors Using Li1.3Al0.3Ti1.7(PO4)3 Reinforced Solid Polymer Electrolyte. *J Energy Storage* **2022**, *49*, 104178. https://doi.org/10.1016/J.EST.2022.104178.

(10) Cheng, Q.; Li, A.; Li, N.; Li, S.; Zangiabadi, A.; Li, T. De; Huang, W.; Li, A. C.; Jin, T.; Song, Q.; Xu, W.; Ni, N.; Zhai, H.; Dontigny, M.; Zaghib, K.; Chuan, X.; Su, D.; Yan, K.; Yang, Y. Stabilizing Solid Electrolyte-Anode Interface in Li-Metal Batteries by Boron Nitride-Based Nanocomposite Coating. *Joule* **2019**, *3* (6), 1510–1522. https://doi.org/10.1016/J.JOULE.2019.03.022.

(11) Yang, F.; Liu, Q.; Xie, W.; Xie, P.; Shang, J.; Shu, X. High-Content Lithium Aluminum Titanium Phosphate-Based Composite Solid Electrolyte with Poly(Ionic Liquid) Binder. *Polymers 2022, Vol. 14, Page 1274* **2022**, *14* (7), 1274. https://doi.org/10.3390/POLYM14071274.

(12) Wang,S; Li, S; Wei, B; Lu,X. Interfacial Engineering at Cathode/LATP Interface for High-Performance Solid-State Batteries. *J Electrochem Soc* **2020**, *167* (10), 100528. https://doi.org/10.1149/1945-7111/AB9A00.

(13) Waetzig, K.; Rost, A.; Heubner, C.; Coeler, M.; Nikolowski, K.; Wolter, M.; Schilm, J. Synthesis and Sintering of Li1.3Al0.3Ti1.7(PO4)3 (LATP) Electrolyte for Ceramics with Improved Li+ Conductivity. *J Alloys Compd* **2020**, *818*, 153237. https://doi.org/10.1016/J.JALLCOM.2019.153237.

(14) Wang, Q.; Yang, A.; Ma, J.; Yao, M.; Geng, S.; Liu, F. Constructing PTFE@LATP Composite Solid Electrolytes with Three-Dimensional Network for High-Performance Lithium Batteries. *Electrochim Acta* **2023**, *467*, 143138. https://doi.org/10.1016/J.ELECTACTA.2023.143138.

(15) Park, C. J.; Na, S.; Park, H. G.; Park, K. Synergistic Effect of Calcination and Sintering on the Reduction of Grain Boundary Resistance of LATP Solid Electrolyte. *ACS Appl Mater Interfaces* **2023**, *15* (22), 26985–26992. https://doi.org/10.1021/ACSAMI.3C04230/SUPPL_FILE/AM3C04230_SI_001.PDF.

(16) Li, J.; He, X.; Yuan, W.; Yu, M.; Wang, X.; Zhang, T.; Luan, L.; Ding, Y.; Sun, H. A Highly Stable Long-Cycle Lithium-Oxygen Battery Based on Flexible PVDF-HFP@LATP Solid-State Electrolyte. *ACS Appl Energy Mater* **2024**, *7* (8), 3484–3496. https://doi.org/10.1021/ACSAEM.4C00536/SUPPL_FILE/AE4C00536_SI_001.PDF.

(17) Anwar, H.; Shahid, H. Bin; Ahmad, H.; Nasir, K.; Ali, Z.; Ali, G. Novel Yttrium and Silicon Co-Doped Li1.3+x+yAl0.3−xYxTi1.7Siy(P1−yO4)3 Solid Electrolyte for Lithium Batteries: Effect on Ionic Conductivity and Crystal Structure. *Energy Storage* **2024**, *6* (4), e628. https://doi.org/10.1002/EST2.628.

(18) Cho, Y.; Le Mong, A.; Hoang, H. A.; Kim, D. Flexible and Hyper Ion-Conductive LATP-Embedded Semi-Interpenetrating Polymer Network Electrolyte Membrane for Solid-State Lithium Battery. *J Energy Storage* **2024**, *92*, 112295. https://doi.org/10.1016/J.EST.2024.112295.

(19) Xu, H. Y.; Fei, G. T.; Xu, S. H.; Chen, W. C.; Li, S. J.; Li, X. F.; Ouyang, H. M. Functional Modification of Polypropylene Separators with Solid Electrolyte LATP and SiO2 Coatings for Lithium Batteries. *Solid State Ion* **2024**, *412*, 116603. https://doi.org/10.1016/J.SSI.2024.116603.